# Insulating phosphoric acid-based geopolymer foams with water and high temperature resistance

Jenny Jouin, J.N. Nouping Fekoua, L. Ouamara, E. Piolet, A. Gharzouni, S. Rossignol

▶ **To cite this version:**

Jenny Jouin, J.N. Nouping Fekoua, L. Ouamara, E. Piolet, A. Gharzouni, et al.. Insulating phosphoric acid-based geopolymer foams with water and high temperature resistance. Construction and Building Materials, 2023, 398, pp.132406. 10.1016/j.conbuildmat.2023.132406 . hal-04264364

**HAL Id: hal-04264364**
**https://hal.science/hal-04264364**

Submitted on 30 Oct 2023

**HAL** is a multi-disciplinary open access archive for the deposit and dissemination of scientific research documents, whether they are published or not. The documents may come from teaching and research institutions in France or abroad, or from public or private research centers.

L'archive ouverte pluridisciplinaire **HAL**, est destinée au dépôt et à la diffusion de documents scientifiques de niveau recherche, publiés ou non, émanant des établissements d'enseignement et de recherche français ou étrangers, des laboratoires publics ou privés.

# Insulating phosphoric acid-based geopolymer foams with water and high temperature resistance

J. Jouin[1,*], J.N. Nouping Fekoua[1,2], L. Ouamara[1], E. Piolet[1], A. Gharzouni[1] and S. Rossignol[1]

[1] *IRCER: Institut de Recherche sur les Céramiques (UMR CNRS 7315), Centre Européen de la Céramique, 12 rue Atlantis, 87068 Limoges Cedex, France.*

[2] *Laboratory of Materials, Local Materials Promotion Authority, MINRESI/MIPROMALO, Yaounde, Cameroon, Po. Box 2396, Yaounde, Cameroon*

[*] *corresponding author: jenny.jouin@unilim.fr*

**Abstract**

This paper aims to determine the feasibility of phosphoric acid-based geopolymer highly porous foams elaborated by a surfactant induced mechanical foaming. The processing and consolidation parameters of the basalt fibers reinforced foams were determined. The influence of the aluminosilicate source on the synthesis of usable samples is reported, showing that the Si/Al ratio as well as the reactivity of the source is crucial to ensure a good consolidation. The effect of the Al/P composition of the geopolymer foam on its properties is also discussed. Two optimal formulations with very good properties (water and temperature resistance, mechanical strength, low thermal conductivity) could be established. Their working properties as well as their main physico-chemical characteristics, allowing to understand their formation mechanism were studied. Both withstood immersion in water and exposition to high temperatures. Their size may also be increased without any difference. Their insulating (61 to 75 $mW.m^{-1}K^{-1}$) and mechanical performances (80 to 190 kPa) are reported, as well as the study of their networks and microstructures.

**Keywords**

Geopolymer, acidic foam, metakaolin, surfactant, thermal conductivity

## I. Introduction

In recent decades, a new category of materials called "geopolymers", belonging to the family of cements and concrete products, has appeared [1]. They result from the dissolution of an aluminosilicate in an activating solution, and then consolidate at relatively low temperatures (less than 100°C), unlike traditional ceramics [2]. The sources of aluminosilicate can come from a variety of clays used in raw or calcined form (argillite, kaolinite, etc.). The most commonly used are metakaolins, which composition, physical and chemical characteristics will strongly influence the reactivity and thus the polymerization reaction [3].This new generation of materials, whether used pure, with fillers or reinforced, has already found applications in many industrial areas, including automotive, aerospace or civil engineering [2].

The geopolymers obtained by the activation from an alkaline solution have been known for many years. Their geopolymerization mechanism has been established in the literature and can be compared to a gel formation [4]. First, the dissolution of the aluminosilicate source takes place by alkaline hydrolysis, and lead to the formation of oligomers. Their reorganization and polycondensation then allows the formation of a three-dimensional tetrahedral network [5] of $SiO_4^{4-}$ and $AlO_4^{5-} + M^+$ with $M^+$ a charge-compensating alkaline cation. In this structure, the tetrahedra are linked together by covalent bonds. More recently, research on geopolymers synthesized by the acid route has been carried out because of their promising properties, especially their high mechanical and high temperature resistances [6]. These materials are synthesized by the activation of the aluminosilicate source by an acid, typically phosphoric acid. After the geopolymerization process, the structure of these amorphous materials seems to be characterized by the strong presence of aluminophosphate networks, and the less prominent signature of silicate, phosphosilicates and hydrated networks [7, 8, 9]. Finally, these materials tend to crystallize at quite low temperature, evolving into a crystalline $AlPO_4$ based matrix, with reported temperatures from 110 to 500°C [8, 10].

Similarly, the formation of geopolymer foams in the alkaline route is well documented [11, 12] and show the high number of applications these bulk materials can be used to. Concerning the foaming process alone, they include different methods, belonging either to chemical or mechanical foaming. The first one is based on the direct formation of bubbles which are trapped in the slurry during its consolidation and is considered as one of the most flexible methods for producing porous monolithic materials [13, 14]. Hydrogen peroxide or fine metallic powders are common foaming agents in this process [15, 16, 17, 18, 19]. Typical density of 0.3 to 0.8 g/cm$^3$, compressive strength from 0.3 to 8 MPa and porosity from 62 to 86 vol% were measured in these materials [20]. The second one consists in the direct addition of foam, which can be previously produced (e.g. prepared by passing air through a diluted surfactant), or foam concentrates, which are then vigorously mixed with the slurry before consolidation [21, 22]. The optimization and combination of the processes lead to very good quality samples with a maximum total porosity of ∼81 vol%, an open porosity of ∼79 vol%, and a compressive strength of ∼3.1 MPa [23, 24].

However, in the case of acid-based route, few works are reported up to now. The formation of foam inside a phosphoric acid activated geopolymer has been achieved by the addition of foaming agents such as aluminum powder [25, 26], hydrogen peroxide [27], iron powder [26], limestone [28] or using Triton X-100 [29]. These new compounds exhibit an excellent thermal stability, high porosity and low compressive strength [25, 27, 29]. In all these materials, in addition to the composition of the material, the mechanical strength and thermal conductivity of geopolymer foams are strongly dependent on the amount of total (open and closed) porosity as well as on the amount of micro- and meso-pores in the matrix (struts and cell walls), the average pore size and its size distribution [11]. Most of the works were performed with chemical foaming and focus on either mechanical performance or thermal conductivity.

In this study, different aluminosilicate sources were tested to develop phosphoric acid-based geopolymer porous materials using an emulsion method to produce the foam. First the existence domains of the samples were established as a function of the chemical formulation. Then the thermal conductivity, mechanical and structural properties of two selected samples were investigated in several conditions such as water immersion, freeze-thaw cycle and high temperature treatment. Finally, the use of these new foams as insulating agents on a larger scale was assessed.

## II. Experimental

### 1 Synthesis

The synthesis of the geopolymer foams was performed using different aluminosilicate sources. More specifically some metakaolins (labeled as $M_2$, $M_3$ and $M_5$ [3]), calcined argillite (denoted as $A_{600}$ and $A_{700}$ [30]) and a laterite clay (L [31]) were selected. The other chemicals used were phosphoric acid (VWR International, Pessac, France, purity 85%), triton CG110 (Dow Chemicals Company), and basalt fibers for mechanical reinforcement. The synthesis was conducted using the following procedure. Firstly, a geopolymer binder was prepared by mixing the aluminosilicate source with phosphoric acid and deionized water. The Al/Si composition was defined by the source, with no modification. The added phosphoric acid corresponded to half of the Al/P of the final composition of the foam (see the compositions of the samples in Figure 1), and the quantity of water was defined to suit the wettability of the aluminosilicate source and ensure the formation of a fluid binder. In parallel, an aqueous foam was prepared with the same amount of water, the remaining part of the phosphoric acid and 4 $\%_{mass}$ of surfactant. The acid + water + surfactant mixture was then vigorously mechanically stirred at 1000 rpm during 15 minutes in order to obtain a low-density aqueous foam. In the final step, 3 $\%_{mass}$ basalt fibers reinforcements were added into the binder reactive mixture, which was finally introduced into the aqueous foam and mechanically stirred. The obtained result was then

kept at 70°C during 4 days in an open mold to ensure the complete solidification of the geopolymer network and the removal of extra water it contained.

## 2 Characterization techniques

The samples were immersed in deionized water with a volume liquid to solid ratio of 25 for 7 days, then the visual aspect of the samples was assessed. The absence of coarse cracks or disaggregation led to classify the samples as water resistant. In addition, a pH-metric monitoring of the water containing the sample was carried out every day in order to identify the eventual dissolution of acidic species. Moreover, the consolidated samples were heat-treated in order to evaluate their resistance to high temperature. They were calcined during 1 hour at 1200°C, with a heating rate of 5°C.min$^{-1}$ and a natural cooling down to room temperature. Finally, the freeze-thaw cycle effect was studied by using a ClimeEvent c/180/73/3 (Weisstechnik, Schunk GmbH) apparatus. The samples were submitted to a repetition of five 20°C / -20°C cycles. The samples in this work are thus labelled as follows: $^{\mathbf{R}}$**S-C**, with **R** being the Al/P ratio, **S** corresponding to the aluminosilicate source ($M_2$, $M_3$, $M_5$, $A_{600}$, $A_{700}$, L) and **C** to the condition applied to the sample (F – freshly synthesized, W – immersed into water, FT – submitted to freeze-thaw cycles, and HT – calcined at 1200°C).

The mechanical resistance of the foams was characterized by compression tests. They were carried out on 20 mm sided cubic samples using an Instron 5969 device equipped with a 5 KN sensor and the Bluehill3 software. The samples were submitted to an increasing load until failure at the speed of 2.5 mm.min$^{-1}$. The thermal conductivity measurements of the samples were carried out using the transient phase source technique using a Hot Disk Transient Plane Source 1500 analyzer [32] equipped with 3.189 mm and 6.403 mm probes, adapted to the size of the samples. The 100 seconds measurements were carried out in transient regime on a homogeneous, isotropic material and of sufficient size to be able to consider it as infinite. The

thermal conductivity measurements were carried out four times on the same and on several samples of the same material to ensure the repeatability of the measurement.

The microstructure of the samples was analyzed via scanning electron microscopy (SEM), using a Quanta 200 FEG FEI microscope. The samples were glued on the sample holder using a silver paste and then coated with a 5 nm layer of Pt.

Fourier-transform infrared (FTIR) spectroscopy spectra of the crushed samples, mixed in KBr, were recorded in transmittance mode on a ThermoFisher Scientific Nicolet 380 infrared spectrometer. The spectra were recorded after 64 scans over a range of 500 to 4000 $cm^{-1}$ with a resolution of 4 $cm^{-1}$. The data were analyzed on the OMNIC software provided by Nicolet Instrument. Samples were also characterized by X-ray diffraction (XRD) on a Bruker D8 Advance diffractometer using CuKα radiation. The data were collected over the 2θ angular range of 10-50° with a step size of 0.02° and an equivalent measured time per step of 50 s. The crystalline phases were identified from the experimental patterns using the powder diffraction file (PDF) database of the International Center for Diffraction Data.

## III. Results and discussion

### 1 Formulation of the foams

#### a. Feasibility

Firstly, the influence of the aluminosilicate source on the formation of foams was investigated. For this, formulations with different sources and Al/Si/P compositions were synthesized; they are represented in the ternary diagram shown in Figure 1. The argillites-based foams were not considered for further analyses, as the consolidated samples could not be manipulated without breaking into pieces. This can be explained by their low content of reactive dehydroxylated aluminosilicate, as identified by Dupuy *et al.* [33, 34]. In this case, the reactive aluminum only exists in small quantities and thus reacts with a very limited part of the phosphor,

leading to an excess of these atoms which inhibits the consolidation [35]. Moreover, according to a previous work by Celerier *et al.* [36], dedicated to dense phosphoric acid-based geopolymers, the Al/Si rich and low P samples tend to consolidate better. This was not the case for argillite-based foams, as represented with the shaded area in Figure 1. The laterite-based foams did belong to the previously identified zone of consolidation. Porous samples could be obtained without the use of metallic powder as described in [31], which validates the process using a mechanical foam alone. The consolidation of these samples relied partly on the presence of impurities [37] such as albite ($NaAl_3Si_3O_{11}$) which, by reacting with the activating solution, modified the polycondensation rections and thus the porous microstructure.

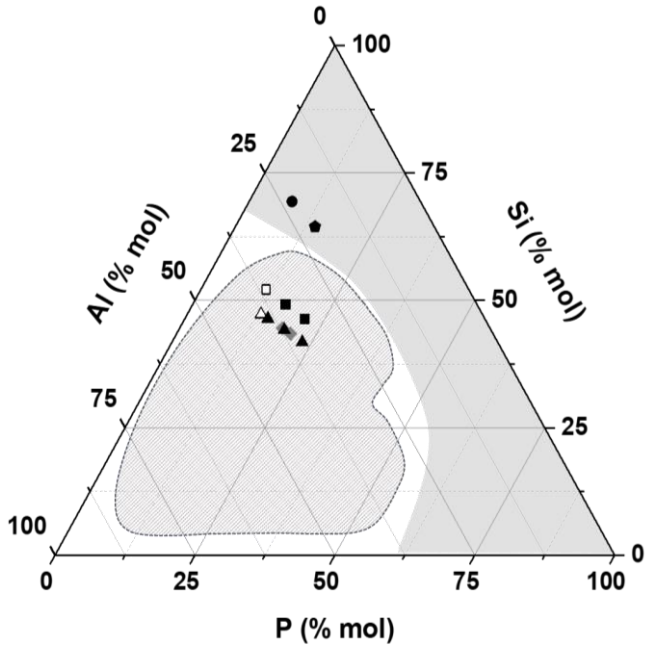


Figure 1: ternary diagram showing the synthesized geopolymer foams, using ▲ $M_2$ (△2.04), ■ $M_5$ (□ 3.10), ● $A_{600}$, ⬟ $A_{700}$ and ◆ laterite. In addition, the hatched (▨) and shaded (▰) zones show the feasibility and non-consolidation zones determined for dense samples [36].

Concerning metakaolins used as aluminosilicates sources, the use of the highly reactive metakaolin $M_3$ was also unsuccessful in this synthesis conditions. In this case, the quick release of both aluminum and silicon atoms within the reaction medium induced the local presence of high concentrations and therefore gradients of chemical potentials inhibiting the quick

formation of Al-O-P network. In the case of $M_2$ and $M_5$ the reactivities of the metakaolins were lower, the Al-O-P networks were created easily [38] and the consolidation of the sample occured before the collapse of the aqueous foam. Moreover, it seems that the crystalline phases contained in the aluminosilicate source act as enhancing sites for geopolymerization by modifying locally the aluminum concentration [39]. It is to be noted that although the synthesized samples can be manipulated, they tend to break easily when cut. To avoid such an outcome, the addition of $3\%_{mass}$ basalt fiber as a mechanical reinforcement in the reactive mixture increased the resistance of the samples. Finally, out of the samples that were prepared, two compositions were selected for further characterizations, as they were the most resistant to manipulations during synthesis and shaping. These two compositions were $^{2.04}M_2$-F and $^{3.10}M_5$-F.

**b. Stability of the samples**

After consolidation, the water, freeze-thaw cycle and high temperature resistances of the selected samples were assessed, the results being shown in Table 1. After one week in water, the foams kept their cohesion with no modification of their visual aspect. The pH value of the immersion water, originally at 6.5, tended to slightly decrease over time, reaching 4.5 for $^{2.04}M_2$-F and 4 for $^{3.10}M_5$-F, respectively. This indicates that a small quantity of acidic species were not strongly bonded to the foam and could migrate into the solution. The samples subjected to freeze-thaw cycles also remained visually unchanged and could still be manipulated after the treatment. Lastly, after the calcination of the samples at 1200°C, apart for a slight modification of the coloration, probably due to the oxidation of the impurities contained in the aluminosilicate source [40], the samples kept their cohesion and remained usable from a mechanical point of view. Overall, all the samples could withstand the different treatments that were applied to them, being water-based, temperature-based or both. The thermal and

mechanical properties of the samples before and after each treatment were thus measured for every configuration.

Table 1: visual aspect of the $^{2.04}M_2$- and $^{3.10}M_5$-based samples after consolidation, water, freeze-thaw and high temperature resistance characterizations. All the represented cubes have a side of 20 mm.

| **Conditions** | **Metakaolin** | |
|---|---|---|
| | **$^{2.04}M_2$-based samples** | **$^{3.10}M_5$-based samples** |
| **Fresh (20°C)** | **$^{2.04}M_2$-F**  | **$^{3.10}M_5$-F**  |
| **Water immersion (20°C)** | **$^{2.04}M_2$-W**  | **$^{3.10}M_5$-W**  |
| **Freeze-thaw cycle (20°C; -20°C)** | **$^{2.04}M_2$-FT**  | **$^{3.10}M_5$-FT**  |
| **High temperature (1200°C)** | **$^{2.04}M_2$-HT**  | **$^{3.10}M_5$-HT**  |

## 2 Mechanical, thermal properties and microstructure

Figure 2 shows the measured compressive stress values as a function of the deformation of the samples based on the compositions $^{2.04}M_2$ and $^{3.10}M_5$. The profiles of the curves are characteristic of composite materials without brittle fracture which is due to the fibers contained in the sample [41, 42]. For lower values of deformation, both formulations display an elastic behavior; this was previously observed in dense geopolymers, although with a higher maximum stress value [43]. The reported compressive strength value for $^{2.04}M_2$-F was 130 kPa, and $^{3.10}M_5$-F exhibited a slightly lower value of 90 kPa, these values being stable after a week-long water immersion or freeze-thaw cycle. After a 1200°C heating cycle, the mechanical behavior is modified for the two compositions. The maximum stress increased slightly, although the general comportment of the sample did not change for $^{2.04}M_2$-HT. The same was observed for $^{3.10}M_5$-HT, with a more brittle behavior in this case. These increases are due to the formation of crystalline species occurring during the thermal treatment [8] and the presence of different amounts of Si-based compounds in the original metakaolins. The values of the compressive strength measured on all the samples are listed in Table 2.

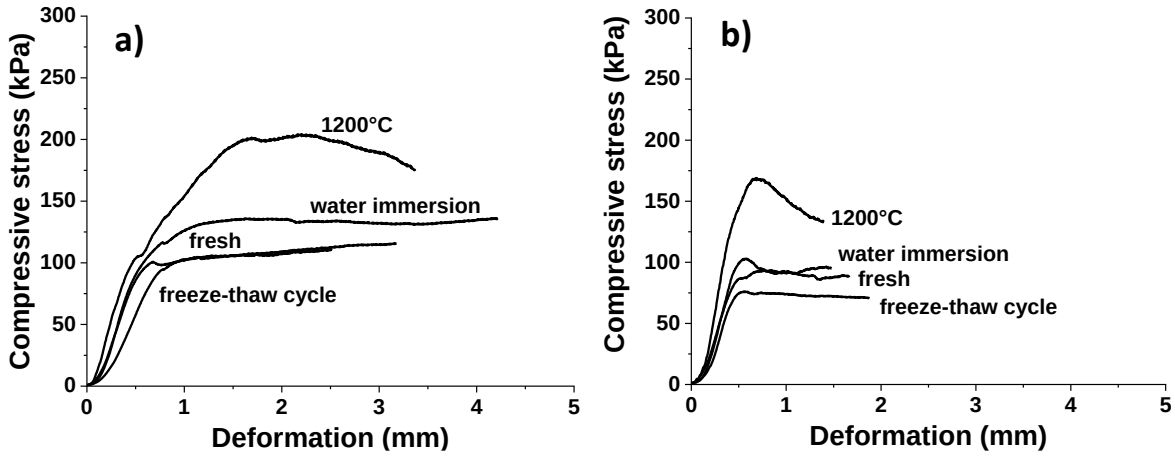


Figure 2: evolution of compressive stress as a function of the deformation for (a) $^{2.04}M_2$-based and (b) $^{3.10}M_5$-based geopolymer foams samples.

The densities of the samples were measured, and are given in Table 2. Whatever the samples, they are relatively low (0.35 to 0.38 g.cm$^{-3}$ for $^{2.04}M_2$-based and 0.46 to 0.50 g.cm$^{-3}$ for $^{3.10}M_5$-based samples), the value usually measured on dense metakaolin-based geopolymers ranging from 1.8 to 2.1 g.cm$^{-3}$ and the density of the fibers being 2.8 g.cm$^{-3}$ [44]. This can be related to the high level of porosity in the samples, which in return can explain the relatively low values of resistance to compressive stress as compared to what is usually measured on dense samples of similar compositions. The reported valued for dense phosphoric acid-based geopolymers indeed range from a few MPa for low phosphorous content, up to 110 MPa for high phosphorous content samples [38].

Table 2: density, thermal conductivity and compressive strength of $^{2.04}M_2$-based and $^{3.10}M_5$-based samples, measured before and after the different resistance treatments.

| **Conditions** | **$^{2.04}M_2$-based samples** | | | **$^{3.10}M_5$-based samples** | | |
|---|---|---|---|---|---|---|
| | **$\rho$ g.cm$^{-3}$** | **$\lambda$ mW.m$^{-1}$K$^{-1}$** | **$\sigma$ kPa** | **$\rho$ g.cm$^{-3}$** | **$\lambda$ mW.m$^{-1}$K$^{-1}$** | **$\sigma$ kPa** |
| **Fresh** | 0.35 | 64 | 130 | 0.46 | 72 | 90 |
| **Freeze-thaw cycle** | 0.37 | 62 | 110 | 0.48 | 74 | 80 |
| **Water immersion** | 0.36 | 61 | 110 | 0.48 | 70 | 90 |
| **High temperature** | 0.38 | 63 | 210 | 0.50 | 75 | 190 |

Similarly, the thermal conductivities (see Table 2) of the samples are low, reaching 61 to 64 mW.m$^{-1}$K$^{-1}$ for $^{2.04}M_2$-based samples and 70 to 75 mW.m$^{-1}$K$^{-1}$ for $^{3.10}M_5$-based samples. The values are not sensitive to the former treatment applied to the samples, which means that the presence of humidity or exposure to high temperature does not degrade the insulating performances of the foams. It is to be noted that in the case of $M_5$-based samples, the slightly higher thermal conductivity could be caused by the presence of iron-based impurities and siliceous species, which might play an important role in the heat conduction.

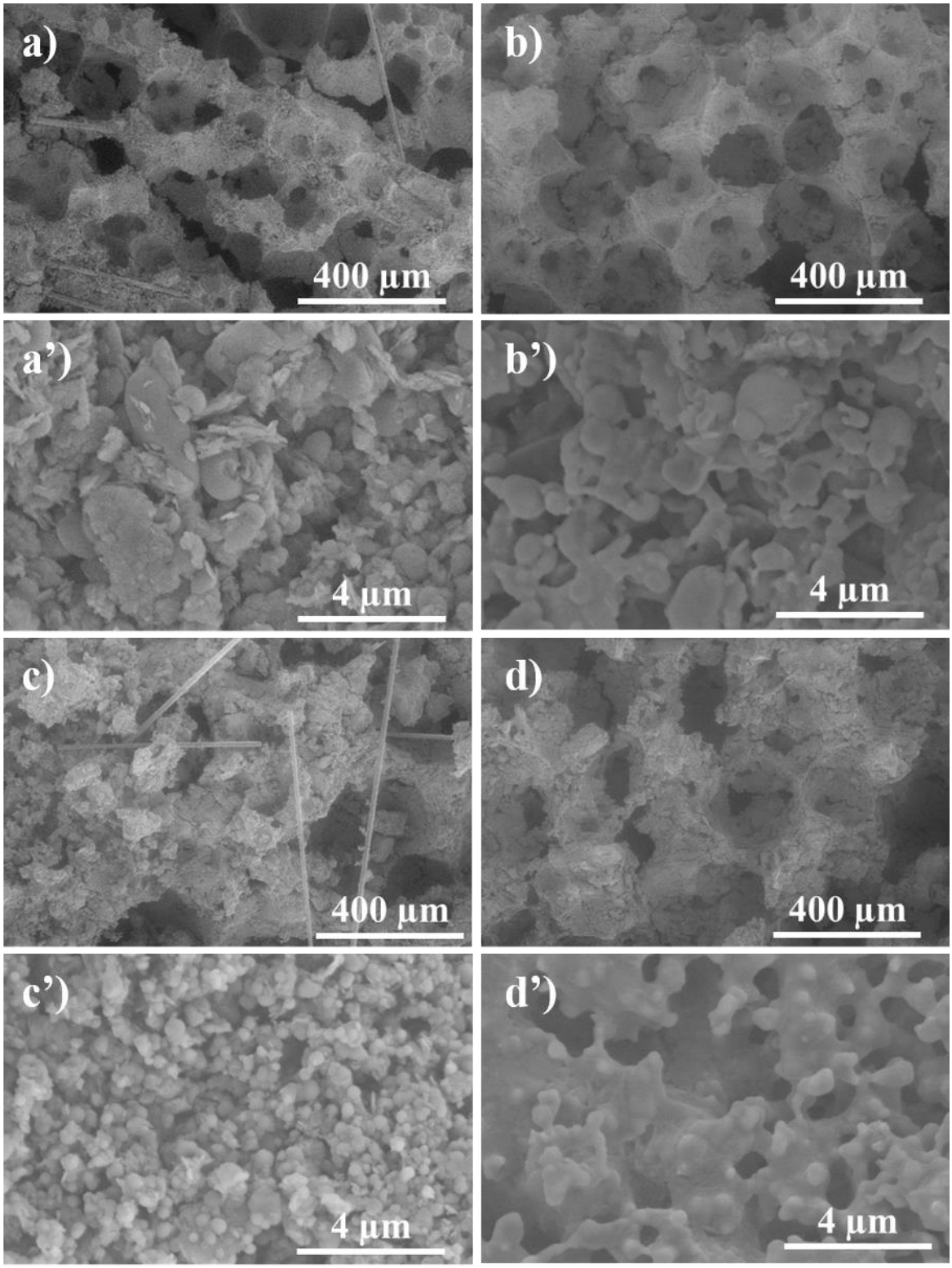


Figure 3: SEM micrographs of (a, a') $^{2.04}M_2$-F (b, b') $^{2.04}M_2$-HT, (c, c') $^{3.10}M_5$-F and (d, d') $^{3.10}M_5$-HT geopolymer foams at low (a, b, c, d) and high (a', b', c', d') magnification.

The microstructures of the $^{2.04}M_2$-F, $^{2.04}M_2$-HT, $^{3.10}M_5$-F and $^{3.10}M_5$-HT samples are presented in Figure 3. The micrographs were used to evaluate the modification of the porosity occurring during heating at high temperature, and to observe the changes in the fine microstructure of the geopolymer skeleton. At room temperature, the low magnification images (Figure 3a and c) reveal the presence of a large number of macropores as well as the random distribution of the basalt fibers visible at room temperature. The size of the pores is up to 300 µm, with the presence of interconnected pores of about 70 µm. This macrostucture was not modified during a heat treatment at 1200°C for both samples, as can be seen in Figure 3b and d. At such temperatures, the fibers are not visible anymore due to their thermal degradation in acidic medium [44]. At a higher magnification, the microstructure of $^{2.04}M_2$-F skeleton (Figure 3a' and b') is characteristic of an acid-based geopolymer [36], with the presence of unreacted metakaolin in the form of small pellets. After a calcination at 1200°C, the small particles are agglomerated, which can be caused by the sintering of the phases. The high magnification images of $^{3.10}M_5$-F (Figure 3c' and d') are similar, although the as prepared sample reveals a more granular structure, typical of agglomerated particles. After a thermal treatment at 1200°C, the particles forming the skeleton seem to be coated in a flow. This could be explained by the presence of a high level of silica and iron oxide in $M_5$, which favors the appearance of a viscous flow [45] at high temperature.

## 3 Structural characterization

### a) As-prepared and room temperature samples

The samples were analyzed by FTIR in order to identify the evolution of their networks under the several room temperature conditions. The spectra of $^{2.04}M_2$-based samples, shown in Figure 4a, display bands at 3700, 3630, 3440, 3350 and 3240 $cm^{-1}$, respectively attributable to ν OH (PO-H) [46], ν OH (Si-O-Si Asym), ν OH (Si-O-Si sym), ν OH ($AlPO_4$) [8] and ν OH

($H_2O$ linked). Then, the two bands at 1640 and 1620 $cm^{-1}$ are respectively due to vibrations δ O-H (PO-H) and δ O-H ($H_2O$). The bands located in the 1200- 900 $cm^{-1}$ range are due to the vibrations of the Si-O-Si and Si-O-Al bonds. [3]. In addition, the bands at 1230 and 1206 $cm^{-1}$ are assigned to ν AlOP and ν SiOP. The presence of the quartz doublet at 797 and 780 $cm^{-1}$ is also observed [47]. No change is detected after the tweeze thaw cycle and water immersion. The same behavior is evidenced in the case of $^{3.10}M_5$-based samples (Figure 4b). Consequently, the same networks are present in the different samples with the existence of a predominant Al-O-P type network, as well as one or more secondary networks based on siliceous and phosphate entities. To sum up this behavior, Figure 4c displays the intensity ratios of some selected bands, representative of the formation of Al-O-P, of a silicate network and a phosphate network (ν Al-O-P, ν Si-O-P and ν P-O), normalized from the band of water at 1620 $cm^{-1}$. The ratio are given as a function of the measured humidity level of the treatment, namely 40% for freshly consolidated, 50% for freeze-thaw cycles and 100% for water immersion. As it can be observed, almost no change is observed with the relative humidity corroborating the networks stability of these samples.

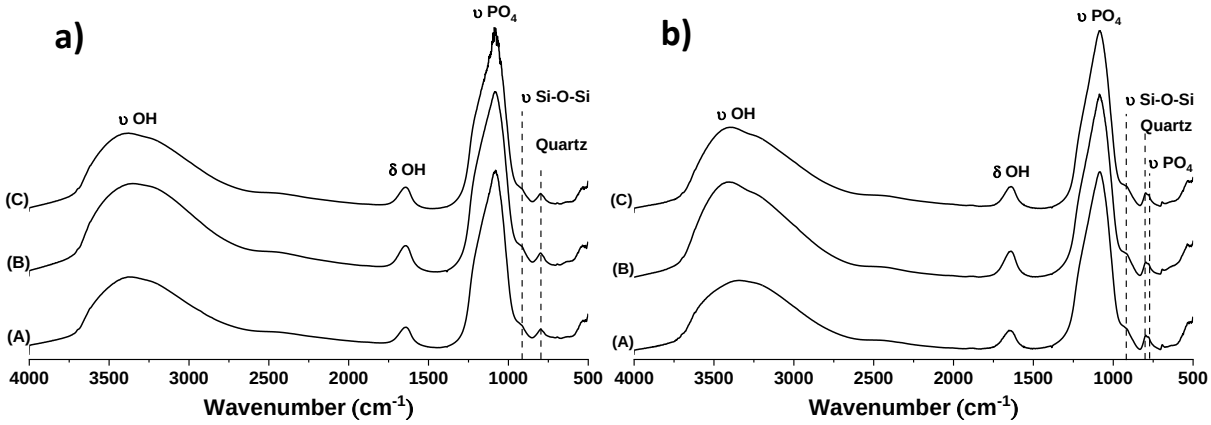

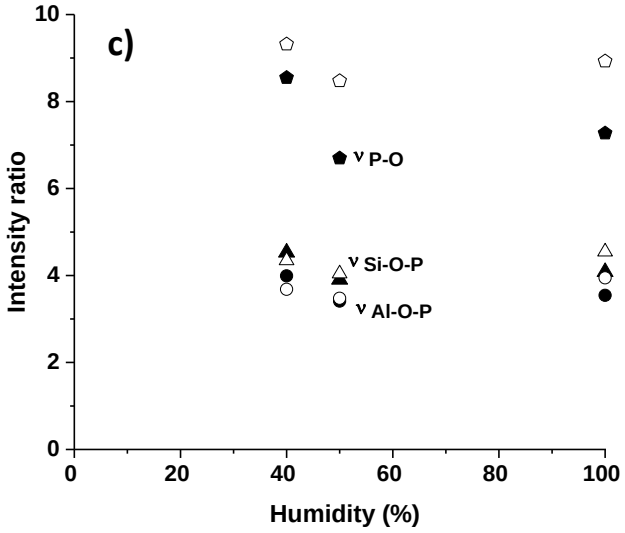


Figure 4: (a) FTIR of (a) $^{2.04}M_2$-based and (b) $^{3.10}M_5$-based geopolymer foams samples under different conditions: (A) fresh, (B) water immersion and (C) freeze-thaw cycle. (c) Relative evolution of the intensities from the different identified contributions as a function of humidity for geopolymer samples (full) $^{2.04}M_2$-based and (empty) $^{3.10}M_5$-based samples. (⬟,⬠) formation of an Al-O-P network, (▲,△) Si-based network and (●,○) P-based network.

The same samples have been analyzed by XRD (Figure 5) in order to identify the crystalline phases that they contained and estimate the evolution of their amorphous networks [8]. On the Figure 5a, $^{2.04}M_2$-based samples show a characteristic dome centered at 24°, indicating the presence of the geopolymer network and remaining Si-based network [36], and various crystallized mineral phases. They were identified as muscovite, quartz and anatase. The same crystalline phases and amorphous contribution have been identified in the different samples, regardless of the treatment applied to them. On the Figure 5b, the diagrams of $^{3.10}M_5$-based samples seem to have a less intense amorphous dome, probably because of the predominance of the quartz-type impurity. Its position is however very close to what can be seen in $^{2.04}M_2$, which points out the relative similarity of the geopolymer networks in these two families of samples. The crystalline phases present in this metakaolin are muscovite, quartz, anatase, mullite and an iron-based compound which has been identified as hematite, giving its red color to $M_5$ [48]. The presence of mullite can be explained by the over-calcination of particles passing

near the flame in the case of flash calcination of kaolin into metakaolin [48]. Again, the same crystalline phases and amorphous dome are found in the different samples.

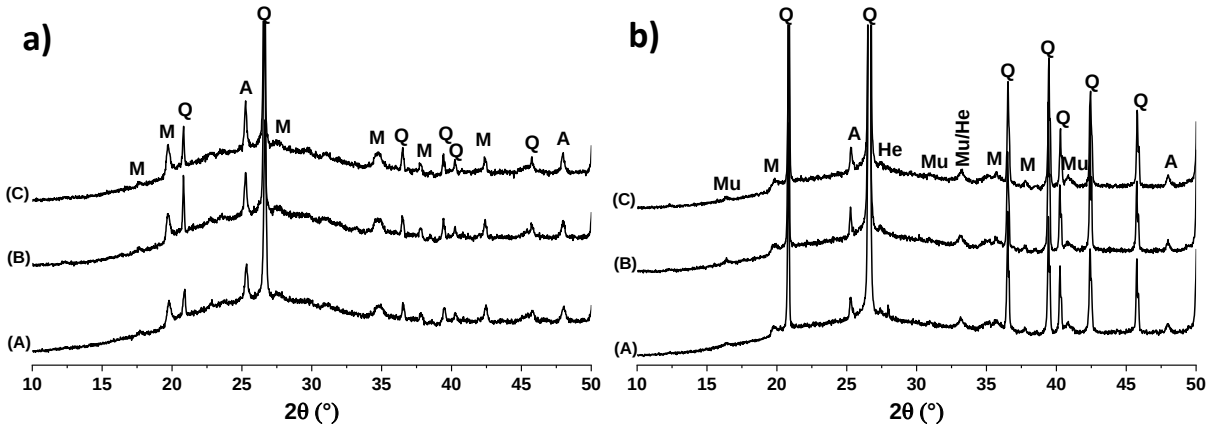


Figure 5: (a) XRD diagrams of (a) $^{2.04}M_2$-based and (b) $^{3.10}M_5$-based geopolymer foams samples under different conditions: (A) fresh, (B) water immersion and (C) freeze-thaw cycle. ((A) anatase, 00-021-1272, (Mu) mullite, 01-079-1456, (M) muscovite, 01-082-3722, (Q) quartz, 01-070-7344, (He) hematite, 01-079-1741)

It would seem that the amorphous phases identified by FTIR and XRD, defined as geopolymer phase and a small amount of amorphous silica, are favorable to a stable network, evolving little with the different room temperature treatments. The crystalline phases are also not sensitive to water-based or freeze-thaw cycles. This stability can account for the lack of difference in the thermal conductivity of the samples before and after resistance treatments. However, when modifying the composition from $^{2.04}M_2$ to $^{3.10}M_5$, the competition between the different networks can explain the observed small increase of the conductivity, as the lower phosphorous content does not allow the formation of the same amount of Al-O-P networks, leading to refractory phases of the $AlPO_4$ type. Also, the presence of crystalline iron-based impurities with higher thermal conductivity is slightly detrimental to the insulating properties of $^{3.10}M_5$-based samples.

**b) Evolution of the structure after a high temperature thermal treatment**

The foam samples were analyzed both by FTIR and XRD after a high temperature treatment to see the formation of crystalline phases from the amorphous networks (Figure 6). The Figure 6a presents the comparative FTIR spectra of the two samples. Both are very similar. For $^{2.04}M_2$-HT, after thermal treatment, the spectrum no longer presents the bands at 1640 and 1620 $cm^{-1}$ respectively attributed to vibrations δ O-H (PO-H) and δ O-H ($H_2O$). In addition, the main contributions centered around 1200 - 800 $cm^{-1}$ are refocused around 1122 $cm^{-1}$. This underlines the crystallization of phases such as mullite or $AlPO_4$ type phases, along with the presence of disordered siliceous entities. More specifically, it can be noted the presence of the bands at 1228 $cm^{-1}$ (ν $PO_4$ in triclinic $AlPO_4$), 1206 $cm^{-1}$ (ν Si-O-P), 1170 $cm^{-1}$ (ν $PO_4$ in berlinite-type $AlPO_4$), 1122 $cm^{-1}$ (ν $PO_4$ in orthorhombic $AlPO_4$), 1095 $cm^{-1}$ (ν $PO_4$), 1070 $cm^{-1}$ (νSi-O-Si/Al), 955 $cm^{-1}$ (νSi-O-Si or amorphous phosphate ion) and 920 $cm^{-1}$ (ν P-OH). The lower frequency bands at 797 and 780 $cm^{-1}$, already seen at room temperature, are due to quartz. The ones at 729 and 710 $cm^{-1}$ are characteristics of ν $PO_4$ in triclinic $AlPO_4$ and ν $PO_4$ in orthorhombic $AlPO_4$, respectively. Finally, two contributions at 692 $cm^{-1}$ (δ O-Si-O) and 669 $cm^{-1}$ (ν Si-O-Si) are due to siliceous entities. The same observations apply for the $^{3.10}M_5$-HT sample, and confirm the crystallization of Al-O-P and Al-O-Si networks, leaving some silicate networks in their original amorphous form.

According to XRD diagrams (Figure 6b), the two samples are crystallized due to the high temperature, and contain the same crystalline phases. The quartz, which was observed in the room temperature samples, is not modified because of its stability up to 1500°C, while the muscovite is not visible anymore. The anatase, which was already in small quantities, was not identified in these samples, although such thermal treatment should not have an influence on this phase. However, with heating, the crystallization of $AlPO_4$ (triclinic and orthorhombic forms) and mullite is observed. The firsts have been previously observed, in particular by

Mathivet *et al.* with the crystallization of the first $AlPO_4$ polymorphs from 110°C [8]. The mullite crystallizes from unreacted metakaolin at 980°C. The probable crystallization of the hexagonal polymorph of $AlPO_4$ (berlinite-type) has been observed in other systems [8, 49] synthesized from amorphous metakaolins. It is difficult to confirm its presence in these diagrams, its diffracting positions being mixed with those of Si-based quartz. Finally, the diagram of $^{3.10}M_5$-HT sample shows peaks which tend to be broader, especially at low intensities. This is typical of the presence of a higher level of structural disorder in the sample.

To summarize, after a thermal treatment at 1200°C, the amorphous part of the samples decreases, and refractory $AlPO_4$-type phases crystallize from the amorphous networks. This has no effect on the thermal conductivity of the samples, which remain low. In the meantime, it slightly increases the compressive strength of the foams, due to the increased rigidity of the crystalline phases as compared to the amorphous networks.

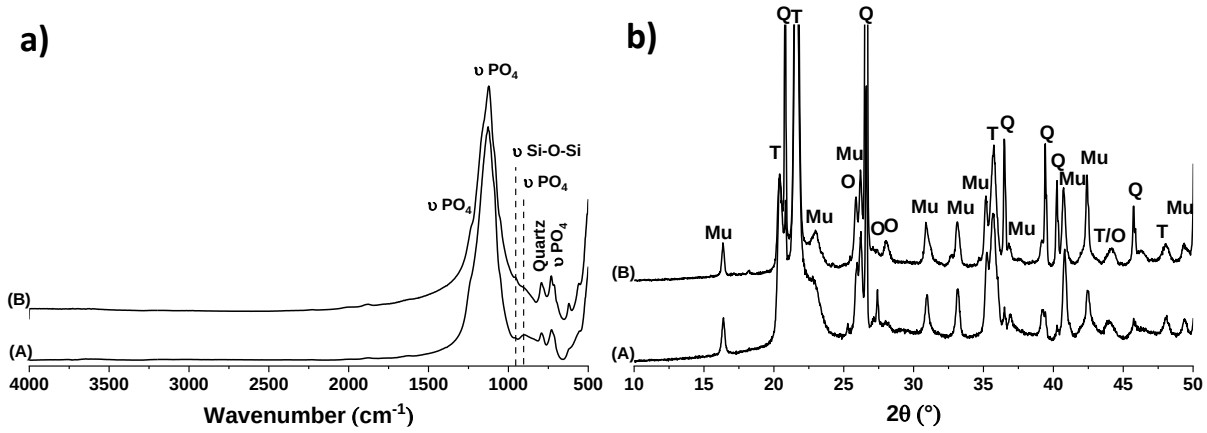


Figure 6: a) FTIR spectra and b) XRD patterns of (A) $^{2.04}M_2$-HT and (B) $^{3.10}M_5$-HT geopolymer foams after thermal treatmant at 1200°C. ((Mu) mullite, 01-079-1456, (Q) quartz, 01-070-7344, (O) orthorhombic $AlPO_4$, 04-014-2298and (T) triclinic $AlPO_4$, 04-012-4467).

## 4 Use as insulating agents

The different results showed that close values of λ and similar mechanical behaviors in temperature were obtained in different water- or temperature-based environments. In this work, phosphoric acid-based foams of thermal conductivity around λ~ 70 $mW.m^{-1}.K^{-1}$ and mechanical strength around σ ~ 100 kPa were indeed produced. All the experimental points were listed in Figure 7 in an Ashby diagram [50] (σ, λ), to compare them with traditional insulating materials, as well as the various data from the literature on both acidic and basic foams. In terms of mechanical and thermal properties, the samples from this study are situated between basic foams obtained either from metakaolin or laterite; the reported values mostly evolve according to the aluminosilicate source.

It should be noted that for foams prepared by an acidic route and using a variety of precursors, higher mechanical values were reported. Using mechanical foaming, compressive strength between 570 and 810kPa were reported after thermal treatments from 25 to 1000°C [29]. Samples prepared by chemical foaming could reach values of 1170 KPa for a content of 2% $H_2O_2$ [27]. Both addition of Al or Fe could strengthen the material by forming crystalline phases and values of 2.6 and 9MPa (for 5% Al and Fe respectively) could be reached [26]. From a thermal conductivity point of view, chemical foaming allowed to reach values between 48 and 161 $mW.m^{-1}K^{-1}$ with hydrogen peroxide as pore forming agent [27]. Tests with limestone also lead to a value of 83 $mW.m^{-1}K^{-1}$ [28]. However, among the literature data few works mentioned both the thermal conductivity and the mechanical resistance, values which were in the same range as the values obtained in this study (48 $mW.m^{-1}K^{-1}$) and 310kPa for the lowest measured thermal conductivity [27]). It seems that the selected process, with the use of emulsion, allows to reach competitive materials in terms of thermal conductivity and thermal resistance.

Finally, for the two compositions, $^{2.04}M_2$-F and $^{3.10}M_5$-F, an increase of the scale of the synthesized foams (up to 35 times of the original samples volume) was successful, indicating a possible upscaling of the process. The obtained foams are represented in Figure 8.

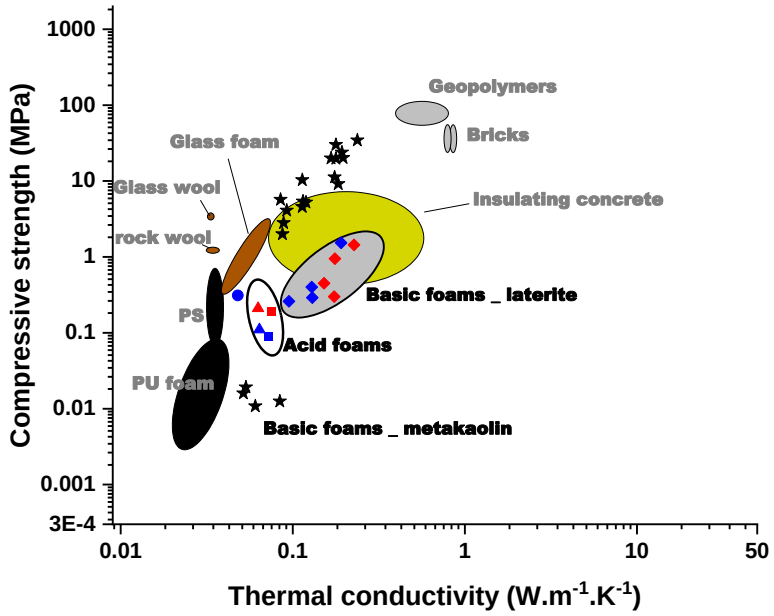


Figure 7: Ashby diagram of (▲) $^{2.04}M_2$-based, (■)$^{3.10}M_5$-based and (●) literature acid-based geopolymer foams samples [27]. Properties of (◆) laterite [31] and (★) metakaolin [51] alkali-based geopolymer foams. The performances of other insulating materials are also given as a comparison. Note: the blue and red dots indicate room temperature and samples treated at 1200°C, respectively.

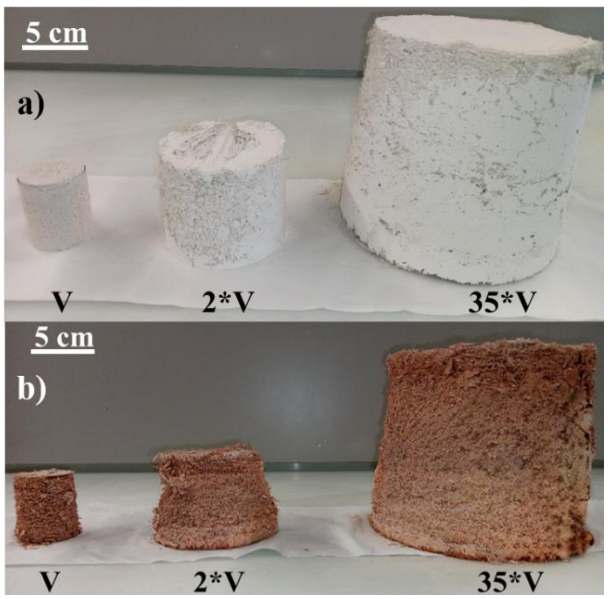


Figure 8: Pictures of (a) $^{2.04}M_2$-F and (b) $^{3.10}M_5$-F geopolymers foams produced with increasing sizes.

## IV. Conclusion

This work was aimed at determining the feasibility of phosphoric acid-based geopolymer foams with a low thermal conductivity and sufficient mechanical resistance. The process was based on the mechanical mixing of a pre-synthesized aqueous foam and a geopolymeric reactive mixture, with the addition of basalt fibers as reinforcements. A selection of aluminosilicate sources was investigated, and the ones most suitable for the final application were selected. Different compositions were synthesized, and led to the establishment of an Al-Si-P-based ternary diagram. This one was coherent with previous observations on dense acid-based geopolymers. Moreover, the upscaling of the process is promising as no difference was evidenced for synthesis volumes up to 35 times the original.

The samples were then characterized, and confirmed the good thermal and mechanical behavior of $^{2.04}M_2$-F and $^{3.10}M_5$-F. All the samples presented water and thermal resistance, which qualifies them as materials usable in different environments. Moreover, the structural and microstructural analyzes illustrated the presence of several amorphous networks in the foams, which are similar before and after room temperature resistance characterizations. After being thermally treated at high temperature, the same phases crystallized in both samples. It seems that the good thermal properties are favored by the presence of a high level of pores, and the example of $^{3.10}M_5$-based foams showed that some impurities tend to decrease these properties even if the geopolymer network is identical. This highlights the crucial importance of the selection and characterization of the aluminosilicate sources in the syntheses.

Finally, these materials are of great interest in the fields of construction for insulation applications but also in the field of refractories to lighten bricks as well as for filtration. The properties measured on the samples synthesized during this work are in line with these expectations.

**References**


[1] J. Davidovits, *Geopolymer Chemistry and Applications*. 4th edition. Saint-Quentin, France, (2015) Institut Géopolymère.

[2] J. Davidovits, *Inorganic Polymeric New Materials* Journal of Thermal Analysis **37** (1991) 1633-56.

[3] A. Gharzouni, E. Joussein, B. Samet, S. Baklouti, S. Rossignol, *Effect of the reactivity of alkaline solution and metakaolin on geopolymer formation*, Journal of Non-Crystalline Solids, **410** (2015) 127-134.

[4] E. Prud'homme, P. Michaud, E. Joussein, A. Smith, C. Peyratout, I. Sobrados, J. Sanz, S. Rossignol, *Geomaterial foams: role assignment of raw materials in the network formation*, J Sol-Gel Sci Technol., **61** (2012) 436-448.

[5] A. Gharzouni, Contrôle de l'attaque des sources aluminosilicates par la compréhension des solutions alcalines, Thesis work, University of Limoges (2016).

[6] H. Celerier, J. Jouin, A. Gharzouni, V. Mathivet, I. Sobrados, N. Tessier-Doyen, S. Rossignol, *Relation between working properties and structural properties from $^{27}Al$, $^{29}Si$ and $^{31}P$ NMR and XRD of acid-based geopolymers from 25 to 1000°C*, Materials Chemistry and Physics **228** (2019) 293-302.

[7] S. Louati, W. Hajjaji, S. Baklouti, B. Samet, *Structure and properties of new eco-material obtained by phosphoric acid attack of natural Tunisian clay*, Applied Clay Science **101** (2014) 60-67.

[8] V. Mathivet, J. Jouin, A. Gharzouni, I. Sobrados, H. Celerier, S. Rossignol, M. Parlier, *Acid-based geopolymers: understanding of the structural evolutions during consolidation and after thermal treatments*, Journal of non crystalline solids **512** (2019) 90-97.

[9] J. Jouin, H. Celerier, L. Ouamara, N. Tessier-Doyen, S. Rossignol, *Study of the formation of geopolymer networks and their resistance to water by time / temperature treatments*, Journal of the American Ceramic Society, **104(10)** (2021), 5445-5456.

[10] W.M. Kriven, J. Bell, M. Gordon, *Microstructure and microchemistry of fully-reacted geopolymers and geopolymer matrix composites*, Ceramic Transactions, **153** (2003) 227-250.

[11] C. Bai, P. Colombo, *Processing, properties and applications of highly porous geopolymers: a review*, Ceram Int **44** (2018) 16103-16118.

[12] R. M. Novais, R. C. Pullar, J. A. Labrincha, Geopolymer foams: An overview of recent advancements, Progress in Materials Science 109 (2020) 100621.

[13] C. Reeb, C. Pierlot, C. Davy, D. Lambertin, *Incorporation of organic liquids into geopolymer materials - A review of processing, properties and applications*, Ceram Int **47(6)** (2021) 7369-7385.

[14] A. Pokhrel, D.N. Seo, S.T. Lee, I.J. Kim, *Processing of porous ceramics by direct foaming: A review*, J Korean Ceram Soc. **50** (2013), 93-102.

[15] J.L. Bell, W.M. Kriven, *Preparation of ceramic foams from metakaolin-based geopolymer gels*, Ceram Eng Sci Proc. **29** (2008), 97-112.

[16] E. Kränzlein, H. Pöllmann, W. Krcmar, *Metal powders as foaming agents in fly ash based geopolymer synthesis and their impact on the structure depending on the Na/Al ratio*, Cem Concr Compos. **90** (2018) 161-168.

[17] E. Prud'homme, P. Michaud, E. Joussein, C. Peyratout, A. Smith, S. Rossignol, *In situ inorganic foams prepared from various clays at low tempera*ture, Appl Clay Sci. **51** (2011) 15-22.

[18] J. Henon, A. Alzina, J. Absi, D.S. Smith, S. Rossignol, *Potassium geopolymer foams made with silica fume pore forming agent for thermal insulation*, J Porous Mater. **20** (2013) 37-46.

[19] H.R. Rasouli, F. Golestani-Fard, A.R. Mirhabibi, G.M. Nasab, K.J.D. MacKenzie, M.H. Shahraki, *Fabrication and properties of microporous metakaolin-based geopolymer bodies with polylactic acid (PLA) fibers as pore generators*, Ceram. Int. **41** (2015) 7872-7880.

[20] S. Yan, F. Zhang, J. Kong, B. Wang, H. Li, Y. Yang, P. Xing, *Mechanical properties of geopolymer composite foams reinforced with carbon nanofibers via modified hydrogen peroxide method*, Mater Chem Phys, **253** (2020), 123258.

[21] M. Strozi Cilla, P. Colombo, Morelli M. Raymundo, *Geopolymer foams by gelcasting*, Ceram Int. **40** (2014) 5723-5730.

[22] J. Stolz, Y. Boluk, V. Bindiganavile, *Mechanical, thermal and acoustic properties of cellular alkali activated fly ash concrete*, Cem Concr Compos. **94** (2018) 24-32.

[23] C. Bai, G. Franchin, H. Elsayed, A. Conte, P. Colombo, *High strength metakaolin-based geopolymer foams with variable macroporous structure*, J Eur Ceram Soc. **36** (2016) 4243-4249.

[24] C. Bai, T. Ni, Q. Wang, H. Li, P. Colombo, *Porosity, mechanical and insulating properties of geopolymer foams using vegetable oil as the stabilizing agent*, J. Eur. Ceram. Soc. **17** (2017) S0955-2219.

[25] L. Le-ping, C. Xue-min, Q. Shu-heng, Y. Jun-li, Z. Lin, *Preparation of phosphoric acid-based porous geopolymers*, J. Applied Clay Science **50** (2010) 600-603.

[26] B.I. Djon Li Ndjock, J. Baenla, E. Yanne, J.B. Bike Mbah, Souaïbou, A. Elimbi, *Effects of Al and Fe powders on the formation of foamed cement obtained by phosphoric acid activation of volcanic ash*, J. Materials Letters **308** (2022) 131147.

[27] Q. Shuai, Z. Xu, Z. Yao, X. Chen, Z. Jiang, X. Peng, R. An, Y. Li, X. Jiang, H. Li, *Fire resistance of phosphoric acid-based geopolymer foams fabricated from metakaolin and hydrogen peroxide*, J. Materials Letters **263** (2020) 127228.

[28] M. Lassinantti Gualtieri, M. Romagnoli, A.F. Gualtieri, *Preparation of phosphoric acid-based geopolymer foams using limestone as pore forming agent - Thermal properties by in situ XRPD and Rietveld refinements*, J. Materials Letters **308** (2022) 131147.

[29] C. Bai, A.Conte, P.Colombo, *Open-cell phosphate-based geopolymer foams by frothing*, J. Materials Letters **188** (2017) 379-382.

[30] A. Gharzouni, C. Dupuy, I. Sobrados., E. Joussein, N. Texier-Mandoki, X. Bourbon, S. Rossignol, *The effect of furnace and flash heating on COx argillite for the synthesis of alkali-activated binders*, Journal of Cleaner Production **156** (2017) 670-678.

[31] J. N. Noupig Fekoua, A. Gharzouni, B. Nait-Ali, L. Ouamara, I. Mbouombouo Ndassa, B. Gouet, E. Kamseu, S. Rossignol, *New laterite-based geopolymer foam resistance under drastic conditions: A comparative study with a metakaolin model*, Ceramics International **49** (2023) 13050-13057.

[32] S.E. Gustafsson, *Transient plane source techniques for thermal conductivity and thermal diffusivity measurements of solid materials*, Review of scientific instruments, **62(3)** (1991) 797-804.

[33] C. Dupuy, A. Gharzouni, N. Texier-Mandoki, X. Bourbon, S. Rossignol, *Alkali-activated materials based on callovo-oxfordian argillite: formation, structure and mechanical properties*, J. Ceram. Sci. Technol., **09(2)** (2018) 127-140.

[34] C. Dupuy, A. Gharzouni, I. Sobrados, N. Texier-Mandoki, X. Bourbon, S. Rossignol, *Thermal resistance of argillite based alkali-activated materials. Part 2: identification of the formed crystalline phases*, Materials Chemistry and Physics **218** (2018) 262-71.

[35] C. Dupuy, J. Havette, A. Gharzouni, N. Texier-Mandoki, X. Bourbon, S. Rossignol, *Metakaolin-based geopolymer: formation of new phases influencing the setting time with the use of additives*, Construction and Building Materials **200** (2019) 272-81.

[36] H. Celerier, J. Jouin, V. Mathivet, N. Tessier-Doyen, S. Rossignol, *Composition and properties of phosphoric acid-based geopolymers*, Journal of Non-Crystalline Solids **493** (2018) 94-98.

[37] P. A. Vallerga, N. Rananandana, *Characteristics of lateritic soils used in Thailand road construction*, Highway Research Record **284** (1969) 85-103.

[38] H. Celerier, J. Jouin, N. Tessier-Doyen et S. Rossignol, *Influence of various metakaolin raw materials on the water and fire resistance of geopolymers prepared in phosphoric acid*, Journal of non crystalline solids, **500** (2018) 493-501.

[39] A. Gharzouni, I. Sobrados, E. Joussein, S. Baklouti, S. Rossignol, *Predictive tools to control the structure and the properties of metakaolin based geopolymer materials*, Colloids and Surfaces A: Physicochemical and Engineering Aspects **511** (2016) 212-21.

[40] P. Scanferla, A. Gharzouni, N. Texier-Mandoki, X. Bourbon, S. Rossignol, *Effects of potassium-silicate, sands and carbonates concentrations on metakaolin-based geopolymers for high-temperature applications*, Open Ceramics **10** (2022) 100257.

[41] N. Ranjbar, M. Zhang, *Fiber-reinforced geopolymer composites: a review*, Cement and Concrete Composites **107** (2020) 103498.

[42] F.U.A. Shaikh, *Review of mechanical properties of short fibre reinforced geopolymer composites*, Construction and Building Materials **43** (2013) 37-49.

[43] D.P. Dias, C. Thaumaturgo, *Fracture toughness of geopolymeric concretes reinforced with basalt fibers*, Cement and Concrete Composites **27(1)** (2005) 49-54.

[44] V. Fiore, T. Scalici, G. Di Bella, A. Valenza, *A review on basalt fibre and its composites*, Composites Part B: Engineering **74** (2015) 74-94.

[45] J. Peyne, *Development of low temperature lightweight geopolymer aggregate, from industrial waste, in comparison with high temperature processed aggregates*, Journal of Cleaner Production **189** (2018) 47-58.

[46] M. Khabbouchi, K. Hosni, M. Mezni, C. Zanelli, M. Doggy, M. Dondi, E. Srasra, *Interaction of metakaolin-phosphoric acid and their structural evolution at high temperature*, Appl. Clay Sci. **146** (2017) 510–516.

[47] N. Essaidi, *Formulation de liant aluminosilicaté de type géopolymère à base de différentes argiles Tunisiennes*, thesis, University of Limoges, 2013.

[48] A. Gharzouni, I. Sobrados, E. Joussein, S. Baklouti, S. Rossignol, *Control of polycondensation reaction generated from different metakaolins and alkaline solutions*, Journal of Ceramic Science and Technology **8(3)** (2017) 365-376.

[49] L. Le-ping, *The phase evolution of phosphoric acid-based geopolymers at elevated temperatures*, Materials Letters **66(1)** (2012) 10-12.

[50] M. F. Ashby, *Choix des matériaux en conception mécanique*, Dunod ed., 2012

[51] M. Arnoult, M. Perronnet, A. Autef, G. Gasgnier, S. Rossignol, *Impact of various aluminosilicate compounds in geopolymer foam formation to a Si/M=0.7 of silicate solution*, Ceramic Engineering and Science Proceedings **38** (2018) 191-200.